Crystal Structure of Rat Apo-Heme Oxygenase-1 (HO-1): Mechanism of Heme Binding in HO-1 Inferred from Structural Comparison of the Apo and Heme Complex Forms[†,‡]

Masakazu Sugishima,[§] Hiroshi Sakamoto,[∥] Yoshimitsu Kakuta,[§,⊥] Yoshiaki Omata,[∥] Shunsuke Hayashi,[∥] Masato Noguchi,[∥] and Keiichi Fukuyama*[,§]

Department of Biology, Graduate School of Science, Osaka University, Toyonaka, Osaka 560-0043, Japan, and Department of Medical Biochemistry, Kurume University School of Medicine, 67 Asahi-machi, Kurume 830-0011, Japan

Received February 11, 2002; Revised Manuscript Received April 8, 2002

ABSTRACT: Heme oxygenase (HO) catalyzes the oxidative cleavage of heme to biliverdin by utilizing O_2 and NADPH. HO (apoHO) was crystallized as twinned $P3_2$ with three molecules per asymmetric unit, and its crystal structure was determined at 2.55 Å resolution. Structural comparison of apoHO and its complex with heme (HO−heme) showed three distinct differences. First, the A helix of the eight α-helices (A−H) in HO−heme, which includes the proximal ligand of heme (His25), is invisible in apoHO. In addition, the B helix, a portion of which builds the heme pocket, is shifted toward the heme pocket in apoHO. Second, Gln38 is shifted toward the position where the α-*meso* carbon of heme is located in HO−heme. Nε of Gln38 is hydrogen-bonded to the carbonyl group of Glu29 located at the C-terminal side of the A helix in HO−heme, indicative that this hydrogen bond restrains the angle between the A and B helices in HO−heme. Third, the amide group of Gly143 in the F helix is directed outward from the heme pocket in apoHO, whereas it is directed toward the distal ligand of heme in HO−heme. This means that the F helix around Gly143 must change its conformation to accommodate heme binding. The apoHO structure has the characteristic that the helix on one side of the heme pocket fluctuates, whereas the rest of the structure is similar to that of HO−heme, as observed in such hemoproteins as myoglobin and cytochromes b_5 and b_{562}. These structural features of apoHO suggest that the orientation of the proximal helix and the position of His25 are fixed upon heme binding.

Heme oxygenase (HO,[1] EC 1.14.99.3), a microsomal enzyme that oxidizes heme to biliverdin IXα, has a key function in physiological heme metabolism (*1*). The reaction pathway of HO consists of three sequential oxidation steps that utilize O_2 and reducing equivalents from NADPH−cytochrome P450 reductase (CPR) (*2*, *3*). In these reaction steps, heme acts as both substrate and cofactor. Three isoforms of HO (HO-1, HO-2, and HO-3) are known in mammals. HO-1 (32 kDa) is expressed at high levels in the spleen and liver and can be induced by various substances, including heme itself. This isoform has been considered to be mainly active in heme catabolism, but recently, it has been suggested that HO-1 is involved in the response to oxidative stress (*4*). In contrast, HO-2 (36 kDa) is expressed constitutively in the brain, testis, and vascular system. The principal role of HO-2 is suggested to be the production of CO as a neurotransmitter (*4*, *5*). HO-3 also catalyzes heme degradation, but its function in vivo has yet to be determined (*6*).

The structures of human and rat HO-1s in a complex with heme have been determined (*7*, *8*). As expected from the high level of sequence homology between the two enzymes, both folds are identical. Rat HO−heme consists of eight helices [Leu13−Glu29 (A), Glu32−Gln38 (B), Arg44−Asn68 (C), Arg86−Tyr97 (D), Pro109−Thr124 (E), Leu129−Met155 (F), Pro175−Met186 (G), and Pro193−Thr222 (H)], and the heme is sandwiched between the A and F helices. The proximal helix, A, provides His25 as the proximal ligand to the heme iron. The distal helix, F, bends at Leu141 and Ser142 so that it is divided into two parts, Leu129−Asp140 and Gly143−Met155 (hereafter termed F-1 and F-2, respectively). Gly139 and Gly143 are the residues closest to the heme at the distal site; the carbonyl group of Gly139 and the amino group of Gly143 are hydrogen-bonded to the water or the hydroxyl anion, which are believed to be the distal

[†] This work was supported in part by Grants-in-Aid for Scientific Research on Priority Areas (Biological Machinery) to K.F. (11169223) and to M.N. (13033041) and for Scientific Research (C) to M.N. (12670125) from the Ministry of Education, Culture, Sports, Science, and Technology of Japan, and Grant 00K1100 from the Ichiro Kanehara Foundation to H.S.

[‡] Coordinates have been deposited in the Protein Data Bank (entry 1IRM).

* To whom correspondence should be addressed. E-mail: fukuyama@bio.sci.osaka-u.ac.jp. Fax: +81-6-6850-5425. Phone: +81-6-6850-5422.

[§] Osaka University.

[∥] Kurume University School of Medicine.

[⊥] Present address: Department of Bioscience and Biotechnology, Graduate School of Bioresource and Bioenvironmental Sciences, Kyushu University, 6-10-1, Hakozaki, Fukuoka 812-8581, Japan.

[1] Abbreviations: apoHO, heme oxygenase; CPR, NADPH−cytochrome P450 reductase; cyt b_5, cytochrome b_5; cyt b_{562}, cytochrome b_{562}; HO, heme oxygenase; HO−heme, heme oxygenase complexed with heme; Mb, myoglobin; NCS, noncrystallographic symmetry; PEG, polyethylene glycol; rms, root-mean-square.

10.1021/bi025662a CCC: $22.00
Published on Web 05/17/2002

ligand to the heme iron. The Pro126−Lys149 stretch, an inner segment of the F helix that includes the two Gly residues, is called the heme oxygenase signature (*9*) and is highly conserved in all HOs thus far investigated.

The incorporation of heme into apoproteins is indispensable for hemoproteins in acquiring biological functions. Although most hemoproteins are unstable in the apo state, some such as myoglobin, cyt b_5, and cyt b_{562} are partially unfolded, yet they have stable secondary and tertiary structures in their apo states. In solution, these apoproteins can be analyzed by various spectroscopic methods; therefore, they are often used as models in studies of heme binding and protein folding (*10*−*12*). HO is not a hemoprotein by nature, but once it binds heme, it behaves like a hemoprotein; the HO−heme complex activates dioxygen and accepts reducing equivalents from CPR (*2*, *3*). It also has spectroscopic features similar to those of myoglobin upon analysis by optical absorption (*13*, *14*), resonance Raman (*13*−*15*), EPR (*13*, *14*), MCD (*16*, *17*), and EXAFS (*16*). As described above, HO−heme primarily consists of α-helices as do many other hemoproteins. The type of folding in HO−heme, however, is not that of globin. Nonetheless, HO-1 (33 kDa, SWISSPROT accession code P06762) shares a number of features with other hemoproteins. Furthermore, HO-1 is larger than sperm whale myoglobin (17.2 kDa, SWISSPROT accession code P00173), rat microsomal cyt b_5 (15.4 kDa, SWISSPROT accession code P16670), and *Escherichia coli* cyt b_{562} (14.1 kDa, SWISSPROT accession code P16670). In this context, clarification of the structure of apoHO should lead to an understanding of the structures of other hemoproteins. In particular, it should help clarify the structural changes caused by heme binding.

We report the crystallization of rat HO-1 (apoHO) and its three-dimensional structure. Rat HO-1 consists of 289 amino acids and has a hydrophobic membrane-binding domain at the C-terminus. Recombinant rat HO-1, in which the C-terminal membrane-spanning region had been truncated (*18*, *19*), was used for the crystallization. Results indicated that the heme pocket of apoHO fluctuates, as has been found for myoglobin (*20*), cyt b_5 (*21*, *22*), and cyt b_{562} (*23*). On the basis of the structural comparison of apoHO and HO−heme, we discuss the mechanism of binding of heme to HO.

MATERIALS AND METHODS

Crystallization of ApoHO. Truncated rat HO-1 (Met1−Pro267) was expressed and purified as described previously (*18*, *19*). We screened the crystallization conditions of apoHO by the use of Crystal Screen (Hampton Research) with the hanging-drop vapor-diffusion method at 277 K. The protein solution was mixed with an equal volume of each reservoir solution and equilibrated against each reservoir solution. Crystals of apoHO were obtained when a reservoir solution containing 2 M ammonium sulfate, 2% PEG 400, 5 mM strontium chloride, and 0.1 M HEPES-NaOH buffer (pH 8.0) was used. The protein concentration used for the crystallization was 20 mg/mL in 20 mM Tris-HCl buffer (pH 7.4) containing ~50 mM KCl. Rod-shaped crystals appeared after 1 day and grew to maximum size in 5 days (Figure 1).

Data Collection and Processing. For cryogenic data collection of the apoHO crystal, it was transferred to the artificial mother liquors, to which ethylene glycol had been added to a final concentration of 12% (w/v). The crystal in the cryoloop was cooled immediately with liquid nitrogen and mounted on the 90° Goniometer Head Arc (Hampton Research) with a nitrogen gas stream at 100 K. Diffraction data were collected at 0.709 Å (λ) and 100 K with synchrotron radiation at beamline BL41XU of SPring-8 equipped with a MarCCD detector. The distance between the crystal and CCD was 222 mm. The crystal was oscillated 2.5° per frame, and the total measurement angle was 150°. The data set was processed, merged, and scaled with MOSFLM (*24*) and SCALA in the CCP4 package (*25*, *26*). The crystallographic data and diffraction statistics are given in Table 1. DETWIN, in the CCP4 package (*25*, *27*), and CNS (*28*) were used to detect crystal twinning and to determine the twinning fraction.

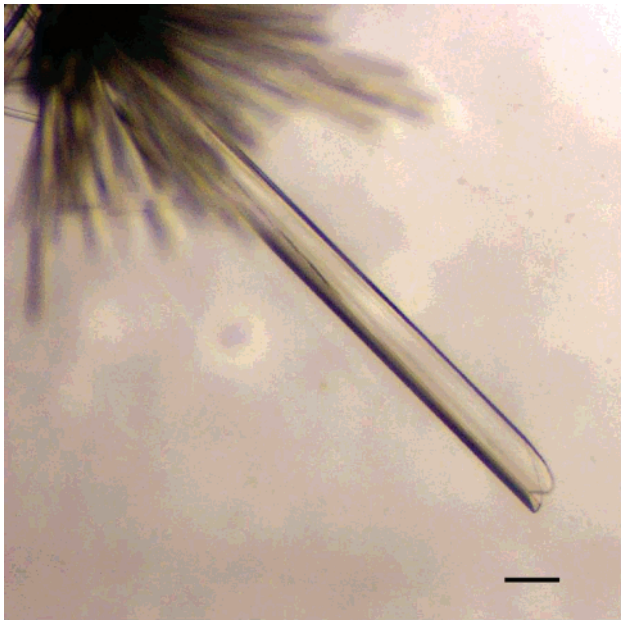

FIGURE 1: Crystal of rat apoHO. The scale bar is 100 μm.

Model Building and Refinement. The apoHO structure was determined by the molecular replacement method with CNS (*28*). The cross-rotation and translation functions were calculated from the rat HO−heme structure (PDB entry 1DVE), from which the heme and water molecules were excluded. The cross-rotation function gave the orientations of the three apoHO molecules present in an asymmetric unit. The subsequent translation function search gave the position of one of the three apoHO molecules in an asymmetric unit. The position of the second molecule was determined by the translation function fixing the position of the first molecule. After the positions of the two molecules were determined, the same process was used to establish the position of the third molecule.

The apoHO crystals obtained in this study were not single but hemihedrally twinned crystals. Britton plot analysis (*29*) and an analysis of the cumulative distribution of H (*27*) were used to determine the twinning fraction. Detwinned data were used in all refinements, the twinning fraction being fixed at 0.45. Test reflections for calculation of the free *R* factor were selected as all the twin-related reflections belonged to the same sets (either the test or working sets) to avoid correlations introduced by twinning (*27*). Because the electron density corresponding to the A helix in the HO−heme

Table 1: Summary of Crystallographic Statistics

Crystallographic Data	
crystal system	trigonal
space group	$P3_2$
unit cell dimensions (Å)	$a = b = 70.2$, $c = 141.5$
no. of molecules in asymmetric unit	3
twinning operator	$k,h,-l$
twinning fraction	0.45
Diffraction Statistics	
resolution (Å)	30.0−2.55
no. of observations	93875
no. of unique reflections	25283
completeness (%)	99.9 (99.9)[d]
mean I/σ	9.9 (2.9)[d]
R_{sym}[a]	0.059 (0.250)[d]
Refinement Statistics	
twinned R/R_{free}[b]	0.202/0.307
detwinned R/R_{free}[c]	0.324/0.394
no. of water molecules	85
average temperature factor (Å^2)	
molecule A	35.1
molecule B	44.6
molecule C	38.7
rms deviations from ideality	
bond lengths (Å)	0.009
bond angles (deg)	1.48

[a] $R_{sym} = \sum_{hkl}\sum_i|I_i(hkl) - \langle I(hkl)\rangle|/\sum_{hkl}\sum_i I_i(hkl)$, where $\langle I(hkl)\rangle$ is the mean intensity for multiple recorded reflections. [b] Twinned $R = \sum|F_{obs}(hkl) - [F_{calc}(hkl)^2 + F_{calc}(kh-l)^2]^{1/2}|/\sum|F_{obs}(hkl)|$. [c] Detwinned $R = \sum|F_{detwin}(hkl) - F_{calc}(hkl)|/\sum|F_{detwin}(hkl)|$. Each R_{free} is the R calculated for 5% of the data set, not including refinements. [d] Values in parentheses are for the outermost shell (2.69−2.55 Å).

structure was not clearly visible after simulated annealing refinement, the A helices of the three molecules in the asymmetric unit were deleted from the model. NCS restraints were applied to the initial refinement and then in subsequent refinements gradually relaxed. NCS restraints were not applied to the final refinement. A few cycles of water picking and conjugate gradient minimization refinements were performed. Temperature factors of all atoms were refined individually. All refinements were carried out using the reflections in the resolution range of 30.0−2.55 Å with CNS (*28*) and using the twinning option. The program O (*30*) was used to adjust and model the protein atoms and water molecules. Stereochemical checks of all the models were made with PROCHECK (*31*). Refinement statistics are given in Table 1.

RESULTS

Determination of the Space Group and Detection of Twinning. Because the apparent diffraction pattern of the apoHO crystal had $P\bar{3}m1$ Patterson symmetry ($R_{sym} = 0.058$) and (00l) diffractions were absent when $l \neq 3n$, we assigned the space group of the crystal as $P3_121$ or $P3_221$. When the space group was assumed to be $P3_221$, two of the apoHO molecules in the asymmetric unit, determined by the molecular replacement method, severely interfered with each other. When the space group of the crystal was assumed to be $P3_2$, the three molecules in the asymmetric unit were favorably packed. In this case, the R and R_{free} factors in the refinements were not decreased ($R/R_{free} = 0.35/0.4$), even though the model was well-fitted to the $2F_o - F_c$ map. The apparent space group of $P3_221$ suggested that the crystal of the $P3_2$ space group may be a perfect twin, with a twinning operator of $k,h,-l$ (*32*). To determine the twinning fraction,

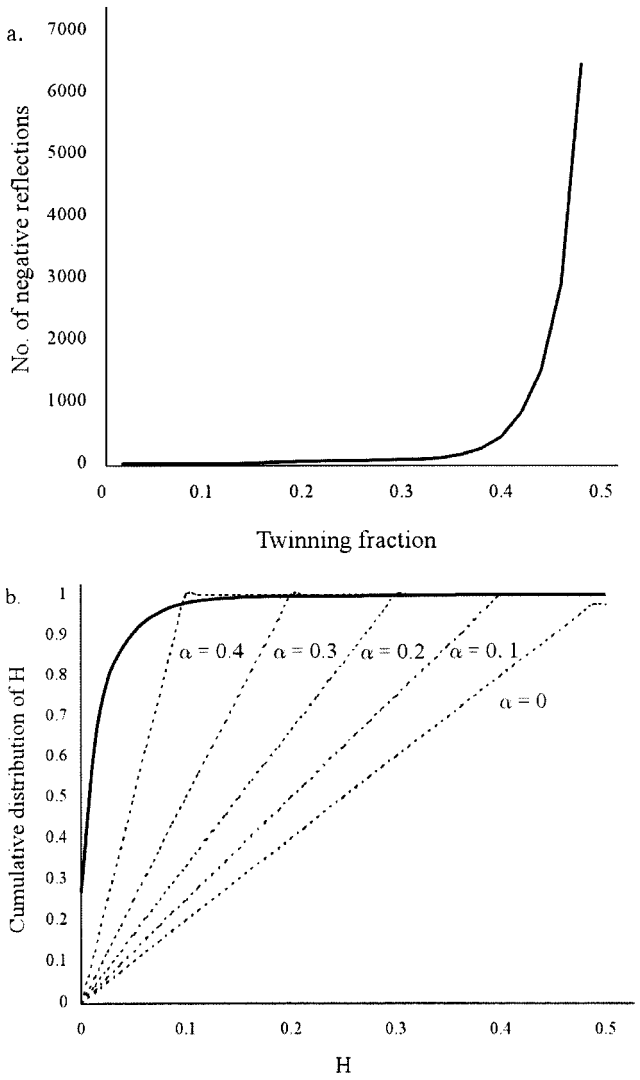

FIGURE 2: Detection of hemihedral twinning and determination of the twinning fraction. (a) Britton plot analysis. The solid line represents the number of negative reflections of the data for apoHO in several estimated twinning fractions. (b) Analysis using the cumulative distribution of H (*31*) for several twinning fractions. The solid line represents the data for apoHO. The twinning operator is $k,h,-l$ in both plots. DETWIN in the CCP4 package (*29*) was used for these plots.

Britton plot analysis (*29*) and a plot of the cumulative distribution of H (*27*) were applied to the diffraction intensity data. Figure 2 shows that this crystal is a twin with a twinning fraction of 0.45.

Because it was a mimetic perfect twinning crystal, we averaged the twin-related reflection intensities to simulate perfect twinning and used these averaged data for refinement on the assumption that the crystal had a perfect twinning (*33*). It should be noted that such refinement procedures were heavily biased toward a Fourier synthesis map from the model. We therefore refined the model with a twinning fraction of 0.45.

Overall Structure. The apoHO structure has been refined to a twinned R factor of 0.202 and a twinned free R factor of 0.307 at 2.55 Å resolution. For statistical reasons, the difference between the R and R_{free} factors in the presence of a twin can be higher than in the usual case (*33*, *34*). There were three molecules (A−C) in the asymmetric unit. The

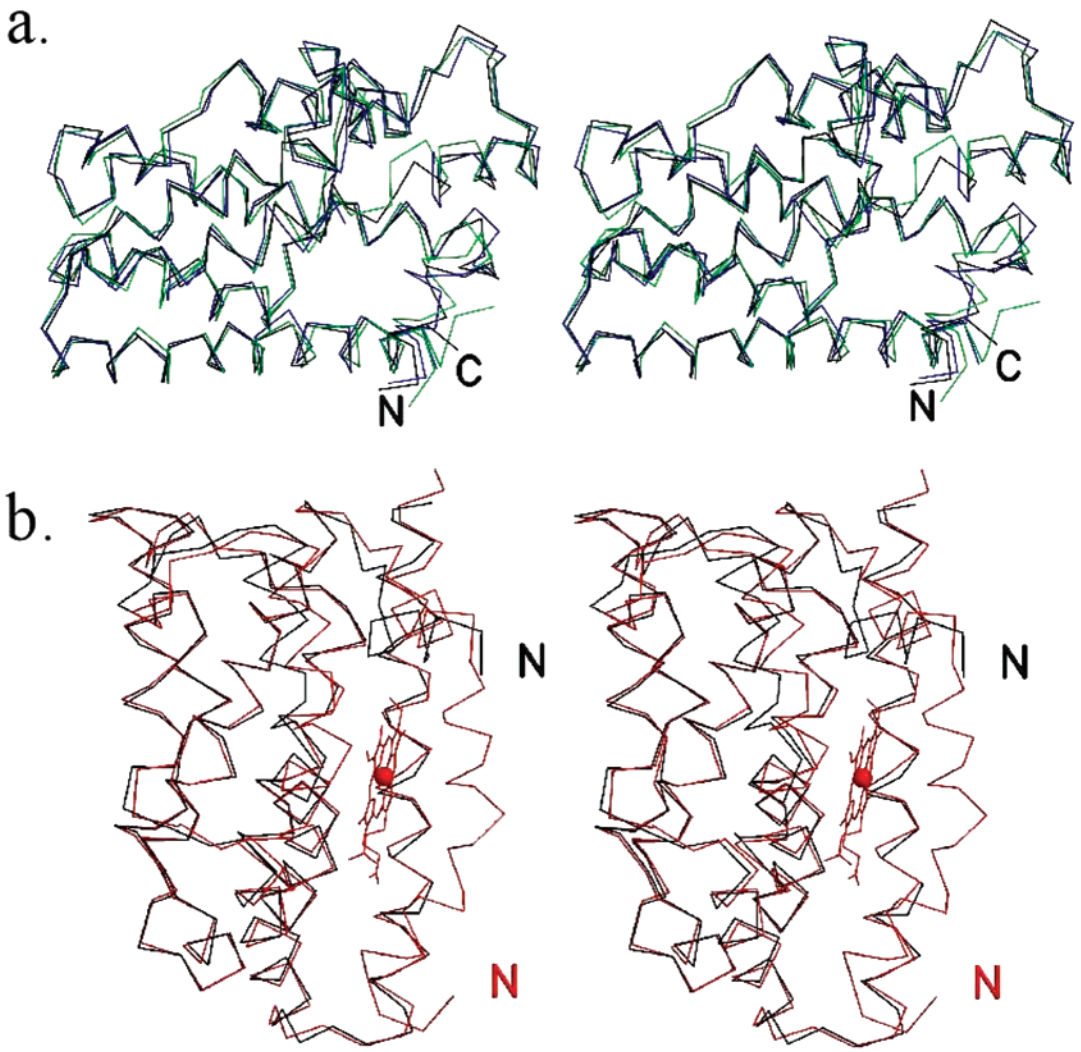

FIGURE 3: Comparisons of three molecules of rat apoHO and HO−heme. (a) Stereoview of the Cα traces of molecules A (black), B (blue), and C (green) of rat apoHO in the asymmetric unit. Superposition was done to minimize the square deviations of the Cα atoms among all the amino acids. The N- and C-termini of the ordered segments are shown as N and C, respectively. (b) Stereoview of the Cα traces of molecule A of rat apoHO (black) and rat HO−heme (red). Superposition was done to minimize the square deviations of the Cα atoms among all the amino acids except the B and F helices. N-Termini of the ordered segments of both molecules are shown in their respective colors as the letter N. This figure was prepared with MolScript (*43*) and Raster3D (*44*).

final model had 4752 protein atoms and 85 water molecules. Approximately 30 N-terminal residues of the 267-residue protein, corresponding to the A helix in HO−heme, were deleted from the model because they were not ordered. The last 40 and several residues were also disordered, as seen in HO−heme. The electron density of molecule B is discontinuous between residues 143 and 144. For molecule A residues 31−222, for molecule B residues 30−142 and 145−223, and for molecules C residues 30−225 could be built.

Superposition of the structures of molecules A−C is shown in Figure 3a. The three molecules have similar folds that mainly consist of α-helices, as evidenced by the low value (0.67 Å) of the overall rms deviation for Cα atoms. The plot of the rms deviations of the apo forms (Figure 4, solid line) shows that residues with a large deviation (>2.0 Å) are localized in the B helix and the B−C loop, and in the middle of the F helix.

A comparison of the overall structure of molecule A of apoHO with that of HO−heme (Figure 3b) shows that the helices that form the heme pocket of HO−heme (i.e., the A, B, and F helices) fluctuate or are distorted in the apo state,

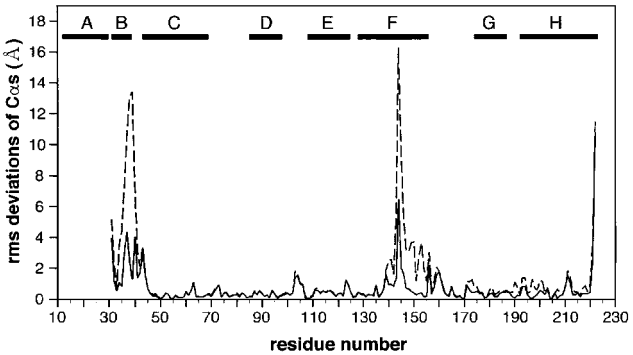

FIGURE 4: Plot of the rms deviations of Cα atoms among apoHOs (solid line) and between apoHOs and HO−heme (dashed line). Solid horizontal bars represent the helices in HO−heme (*8*).

whereas the remainder of the apoprotein, including the C−E, G, and H helices, has essentially the same packing conformation as that of HO−heme. When the rms deviations of the Cα atoms were calculated by combining the data sets for HO−heme and apoHOs (Figure 4, dashed line), residues in the B helix, B−C loop, and in the middle of the F helix

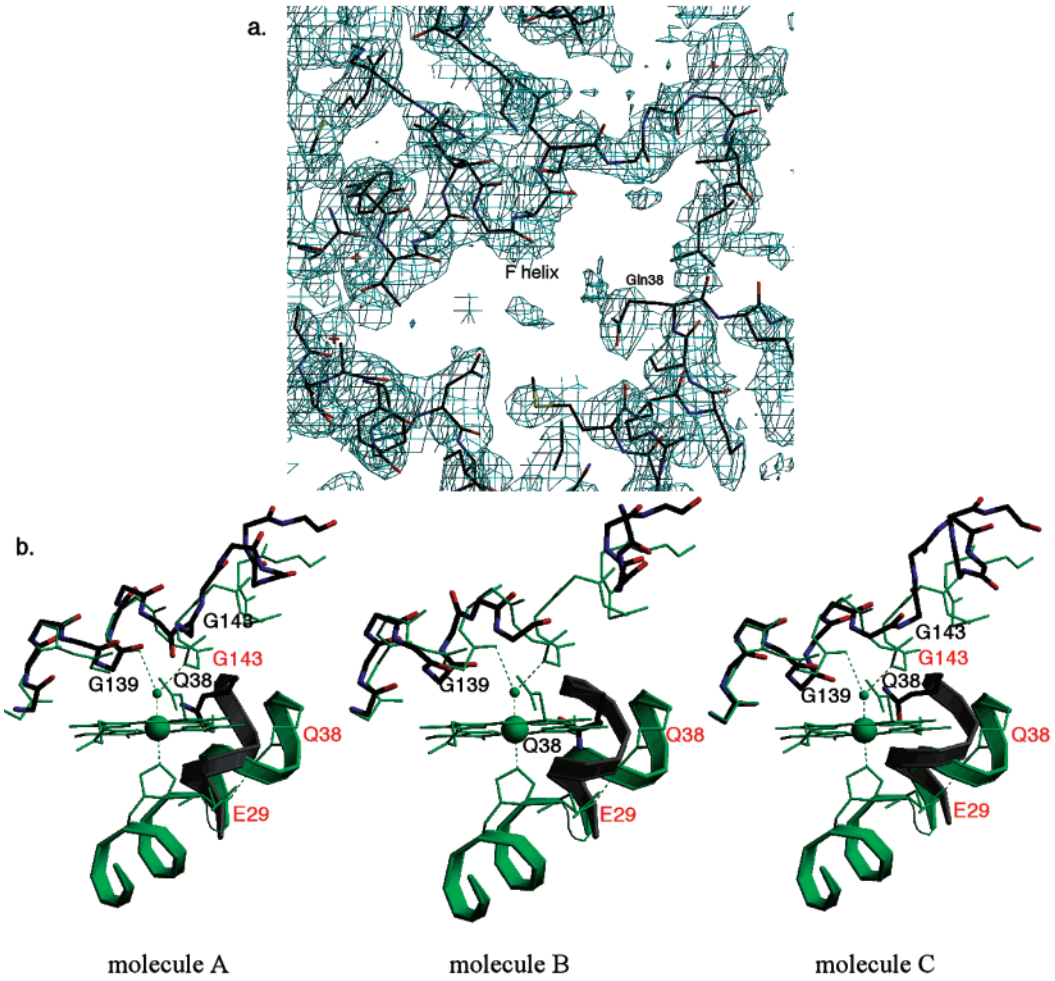

FIGURE 5: Structural comparisons between apoHO and HO−heme. (a) Sigma-A-weighted $2F_o - F_c$ map contoured at 1.3σ (cyan) superimposed on the wire-frame model of molecule C of apoHO around the heme pocket. (b) Superpositions of the models near the heme pocket of apoHO (carbon, black; oxygen, red; nitrogen, blue) and rat HO−heme (green). Both molecules are shown as wire-frame models. Dashed lines represent hydrogen bonds or coordinate bonds. This figure was prepared with MolScript (*43*) and Raster3D (*44*).

had larger values than those calculated for apoHOs. In addition, the deviation increased for the residues in F-2. The greatest part of the variance between the apo- and holoproteins therefore is localized around the heme pocket.

Distal Helix. An electron density map of molecule C around the heme pocket is shown in Figure 5a. In HO−heme, the F helix covers the distal surface of the heme, with closest access of Gly139 and Gly143 to a water or hydroxyl ligand (*8*). In contrast, the F helix in apoHO, especially at the F-2 segment, shifts away from the heme pocket, although it remains bent (Figure 5b). The conformation of a few residues around Gly143 changes from an α-helix to a random coil. The amide group of Gly143 in molecule A is directed away from the heme pocket, whereas the carbonyl group of Gly139 still points in the same direction as that in HO−heme. The F helix in molecule B fluctuates markedly, Gly143 and Gly144 being disordered. In molecule C, the F helix adopts a conformation similar to that in molecule A, but the position of Gly139 is altered for its carbonyl group to turn aside from the heme pocket.

Proximal Side. In addition to the disorder of the A helix in apoHO, the B helix shifts toward the heme pocket, accompanied by several conformational changes in the side chains of its amino acid residues. For example, in HO−heme, Nε of Gln38 is hydrogen-bonded to the carbonyl oxygen of the backbone of Glu29 at a distance of 2.9 Å, but in apoHO, Nε of Gln38 of molecule A is located near the position where the α-*meso* carbon of the heme originally was present in HO−heme. The Gln38s of the other molecules also shift toward the heme position. They are not near the α-*meso* carbon; rather they are closer to (molecule C) or occupy (molecule B) the position of the heme in HO−heme (Figure 5b).

In HO−heme, Lys179 and Arg183 interact electrostatically with the propionate group of the heme (*7*, *8*). The Arg183 of the three apoHO molecules and the Lys179 of molecule C of apoHO have approximately the same conformations as those in HO−heme (Figure 6), but the side chains of Lys179 in molecules A and B are flipped at the Cβ atom. As a result, Lys179 Nζ more closely approaches the position at which the propionate group of the heme originally was present in HO−heme (Figure 6). In HO−heme, Met34, Phe37, and Phe214 form a hydrophobic wall opposite the α-*meso* heme edge (*7*, *8*). These apoHO residues roughly retain their conformations, but Met34 and Phe37 approach the inside of the heme pocket due to the B helix shift. In particular, the Phe37 in molecule B is much closer to the position of the heme in HO−heme than is the Phe37 of the other apoHO molecules (Figure 6). The side chain of Phe207, present under the β-*meso* edge of the heme (*7*, *8*), is flipped at the

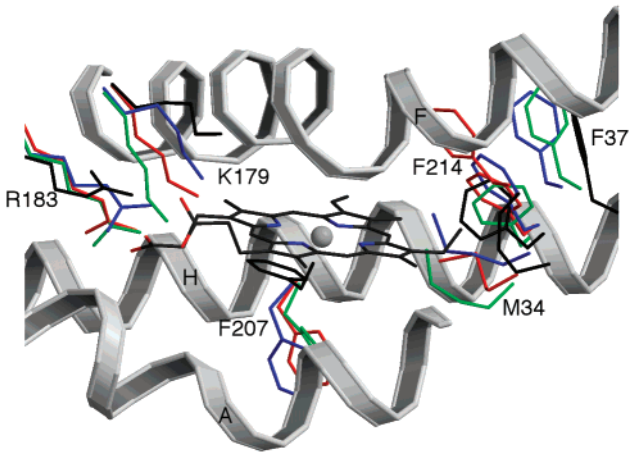

FIGURE 6: Structural changes in the hydrophobic and electrostatic interactions between HO and heme. Ribbon diagrams and wire-frame models of heme and the side chains of Met34, Phe37, Lys179, Arg183, Phe207, and Phe214 of rat HO−heme (black) are shown. The side chains of molecule A (green), molecule B (red), and molecule C (blue) of apoHO are superimposed on HO−heme. This figure was prepared with MolScript (*43*) and Raster3D (*44*).

Cβ atom and points down toward the position of the A helix in HO−heme (Figure 6). As a result, the fluctuations and distortions in apoHO lead to the exposure of the heme binding pocket to solvent. The heme pocket of apoHO therefore should be more easily accessible for heme binding.

Core Structure. The Cα atoms of residues 44−138 and 155−220 in apoHO can be superimposed on the Cα atoms of the corresponding residues in HO−heme with a low rms deviation of 0.55 Å, indicating there is little change in the core structure of HO whether heme is present. An extended hydrophobic cluster is formed along the interfaces of the C, E, F-1, and H helices (Figure 7a). Aliphatic and aromatic residues of the two loops between the C and D helices and between the F and G helices also participate in this hydrophobic interaction. The D and G helices exist outside of the core, but both establish van der Waals contacts with the C helix and the first half of the F helix, respectively, by forming hydrophobic interfaces. In addition to these hydrophobic interactions, both the helix−helix and helix−loop interfaces are stabilized by a number of hydrogen-bonded or electrostatic pairs: Tyr58 and Asp140, Glu62 and Arg86, Glu66 and Tyr78, Trp96 and Gly163, Arg117 and Glu202, Arg198 and Glu127, Asn210 and Arg136, Glu216 and Thr108, and Glu216 and Ala110 (Figure 7b).

Like HO−heme, the surface of the heme-binding side of apoHO is charged positively and the opposite one negatively. This feature is important for interaction with CPR. The surface charge distribution of apoHO is essentially the same as that of HO−heme. CPR therefore would contact HO even in the apo state, but it remains to be explained how this interaction is involved in heme oxygenase catalysis.

DISCUSSION

The major differences in the crystal structures of HO−heme and apoHO are limited to the helices directly involved in heme binding. The proximal helix, A, in apoHO is not visible in this analysis. The distal helix, F, partially fluctuates; its middle portion becomes a random coil, and the latter half (Val146−Ala151) varies in conformation among the three apo forms. In contrast, both helices in HO−heme are

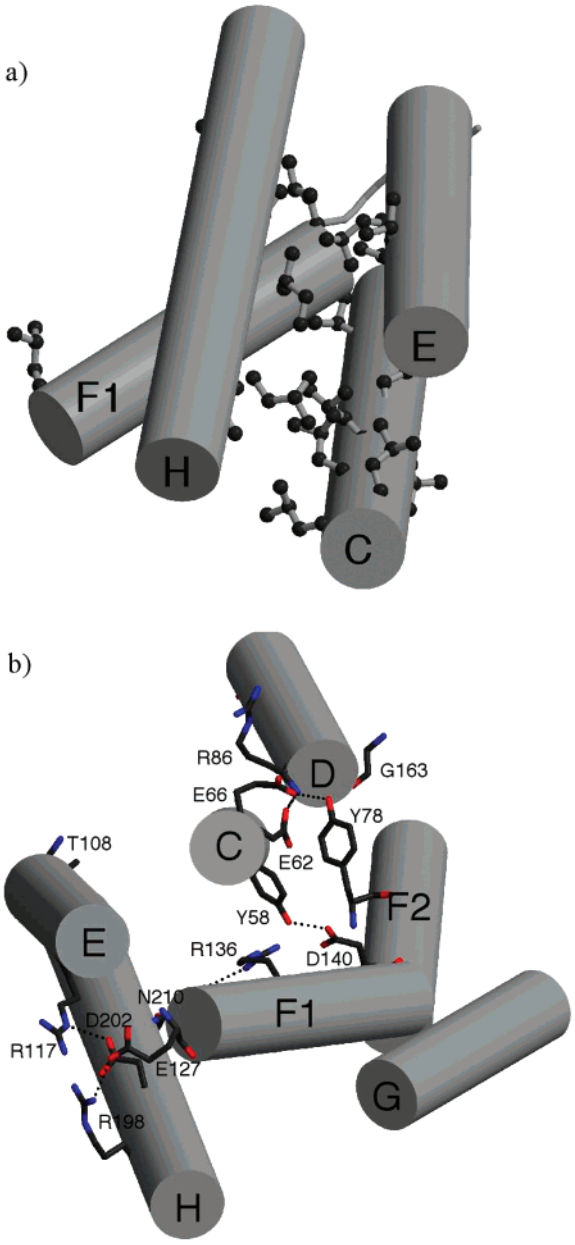

FIGURE 7: Schematic representations of the core structure of apoHO. (a) The hydrophobic core of HO is shown. The C, E, F-1, and H helices are shown as cylinders. Hydrophobic residues (Leu, Ile, and Val) in these helices are shown as ball-and-stick models. (b) C−H helices in apoHO are shown as cylinders. Hydrogen bonding and electrostatic interactions conserved among the rat HO−heme and apoHOs are represented with dotted lines. Side chains involved in these interactions are shown as wire-frame models. This figure was prepared with MolScript (*43*) and Raster3D (*44*).

stabilized by a number of interactions with heme, i.e., coordination of the imidazole side chain of the proximal His25 to the heme iron, an electrostatic interaction between the NζH_3^+ group of Lys18 and the propionate groups of the heme, and the hydrogen bonds between the backbones of the distal glycines and the distal water ligand of the heme. Other electrostatic interactions occur between the basic side chains of Lys179 and Arg183 and the propionate groups of heme. These electrostatic interactions present in rat HO-1 are also conserved in human HO-1 (*7*). Interestingly, the mutation of Arg183 to Glu or Asp was found to cause changes in the α-regioselectivity of the heme oxygenase reaction (*35*). It is noteworthy that the basic side chains of

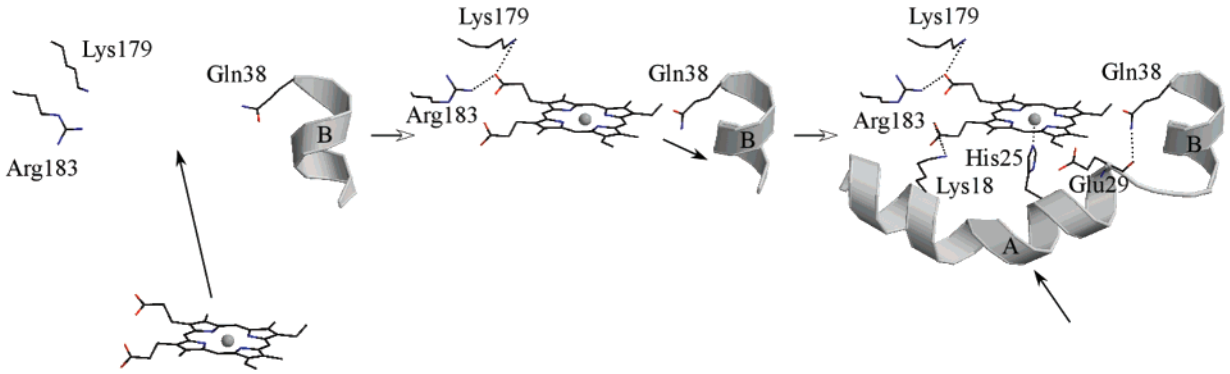

FIGURE 8: Proposed mechanism of heme binding to apoHO. This figure was prepared with MolScript (*43*) and Raster3D (*44*).

Lys179 and Arg183 in apoHO maintain an orientation similar to those in the holo state. Furthermore, in the holoprotein, a hydrogen bond between the backbone of Glu29 in the A helix and the side chain of Gln38 in the B helix appears to contribute to the formation of the heme pocket. A previous study showed that replacement of the proximal His25 with Ala led to the loss of HO activity, but this substitution did not significantly affect the molecule's heme binding capability, indicative that these stated additional interactions, rather than the coordination of His25 to heme, are crucial in the initial stage of heme binding (*36*).

When all these findings are considered, they suggest a possible induced-fit model for the binding of heme to HO (Figure 8). Before heme binding, the A helix assumes a random conformation such that the heme pocket is exposed to the solvent. The side chain of Gln38 partially occupies the binding site. Once heme binds to the heme pocket, Gln38 and the B helix shift away from the pocket to avoid steric hindrance between the heme and Gln38. The electrostatic interaction between the propionate groups of heme and the side chains of Lys179 and Arg183 would facilitate the correct orientation of the heme. Gln38 Nϵ then forms a hydrogen bond to Glu29 O of the A helix, and the angle between the A and B helices is fixed. Finally, Lys18 and the propionate groups of the heme form a salt bridge, and His25 Nϵ ligates to the heme iron. The structural features of the heme pocket are well-conserved in rat and human HO-1s, suggesting that mammalian enzymes use a similar mechanism to incorporate the heme substrate.

Recently, the crystal structure of the *Neisseria meningitidis* HO in complex with heme was determined (*37*). Gln38 is conserved among mammalian HO-1s, but is substituted for Val in *N. meningitidis* HO. This substitution suggests that the binding mechanism of the heme of *N. meningitidis* HO may differ somewhat from that in our proposed model (Figure 8). In *N. meningitidis* HO−heme, there is a C-terminal loop at the position where the B helix is in HO-1−heme. The A helix should be stabilized by the interaction between the A helix and the C-terminal loop via hydrogen bonding (Asp28 Nδ−Met208 O) in *N. meningitidis* HO−heme. In mammalian HO-1s, the segment which corresponds to the C-terminal loop in the *N. meningitidis* HO−heme is disordered, but its structure probably differs from that of the *N. meningitidis* HO−heme because there is no sequence similarity between the mammalian HO-1 and *N. meningitidis* HO in this region. Mammalian HO-1s are membrane-bound proteins that span the membrane of the endoplasmic reticulum at the C-terminus, and *N. meningitidis* HO is a soluble protein (*38*). This difference is thought to be responsible for the structural difference at the C-termini.

The kinking and flexibility of the distal helix are believed to be crucial factors for heme oxygenase catalysis. An asymmetric unit of human HO−heme crystals has "closed" and "open" forms, which differ in the distance between the distal helix and heme plane (*7*). The opening of the active site has been inferred to allow substrate binding and product release, while the closing of this site would enforce regioselectivity and facilitate the reaction. In apoHO, the three molecules in the asymmetric unit have different conformations in the segment that corresponds to the F-2 segment in HO−heme. Moreover, a few residues around Gly143 have changed their secondary structures to a random coil, an indication that this segment forms an unstable conformation in apoHO. The flexibility of this segment differs from that at the kinked site (Leu141−Ser142), causing an overall shift of the F-2 segment as seen in the structures of HO−heme complexes (*7*, *8*, *37*). The primary factor that determines the flexibility in apoHO probably is the absence of heme because this segment has direct contact with the heme plane, and the distal ligand of the heme iron is hydrogen-bonded to Gly143 in rat HO−heme (*8*). Unlike the proximal and distal helices, the remainder of HO retains its structure, irrespective of whether heme is bound. Five helices (C−E, G, and H) and part of the F helix assemble to form the extended hydrophobic core. This core structure most likely provides stability for the overall structure of the enzyme, thereby minimizing conformational change on both binding of the substrate and release of the product.

It should be noted that, consistent with the structure of apoHO, the known structures of the apoproteins cyt b_5 (*21*, *22*) and cyt b_{562} (*23*) have a similar feature in common; one of the axial helices fluctuates greatly, whereas the other remains folded. Studies of several apoMb properties have indicated that apoMb is in the molten-globule state (*39*) and that one side of its heme pocket (F helix) is disordered (*20*). Although HO, Mb, cyt b_5, and cyt b_{562} exhibit similar structural changes around the heme pocket upon heme binding, there is no similarity in their overall structures; HO (*7*−*9*), Mb (*40*), and cyt b_{562} (*41*) are all α proteins with different folding motifs, and cyt b_5 (*42*) consists mainly of antiparallel β-sheets and α-helices. This finding suggests that there is a common feature between the pathways to maturation of the three *b*-type hemoproteins and the heme binding in HO. Heme is inserted into the opened heme pocket of the apoprotein, fixes the orientation of the disordered helix, and stabilizes the conformation of the heme pocket.

ACKNOWLEDGMENT

We thank Dr. Masahide Kawamoto of the Japan Synchrotron Radiation Research Institute (JASRI) for his valuable help with data collection using the synchrotron radiation of BL41XU, SPring-8. The synchrotron radiation experiments were performed at SPring-8 with the approval of JASRI (Proposals 1999B0201-NL-np and 1999B0389-CL-np).

REFERENCES

1. Tenhunen, R., Marver, H. S., and Schmid, R. (1968) *Proc. Natl. Acad. Sci. U.S.A. 61*, 748−755.
2. Yoshida, T., Noguchi, M., Kikuchi, G., and Sano, S. (1981) *J. Biochem. 90*, 125−131.
3. Yoshinaga, T., Suto, Y., and Sano, S. (1990) *Biochem. J. 270*, 659−664.
4. Prabhakar, N. R. (1998) *Respir. Physiol. 114*, 57−64.
5. Prabhakar, N. R. (1999) *Respir. Physiol. 115*, 161−168.
6. McCoubrey, W. K., Jr., Huang, T. J., and Maines, M. D. (1997) *Eur. J. Biochem. 247*, 725−732.
7. Schuller, D. J., Wilks, A., Ortiz de Montellano, P. R., and Poulos, T. L. (1999) *Nat. Struct. Biol. 6*, 860−867.
8. Sugishima, M., Omata, Y., Kakuta, Y., Sakamoto, H., Noguchi, M., and Fukuyama, K. (2000) *FEBS Lett. 471*, 61−66.
9. Maines, M. D. (1988) *FASEB J. 2*, 2557−2568.
10. Privalov, P. L. (1996) *J. Mol. Biol. 258*, 707−725.
11. Banci, L., and Presenti, C. (2000) *J. Biol. Inorg. Chem. 5*, 422−431.
12. Kamtekar, S., and Hecht, M. H. (1995) *FASEB J. 9*, 1013−1022.
13. Takahashi, S., Wang, J., Rousseau, D. L., Ishikawa, K., Yoshida, T., Host, J. R., and Ikeda-Saito, M. (1994) *J. Biol. Chem. 269*, 1010−1014.
14. Sun, J., Wilks, A., Ortiz de Montellano, P. R., and Loehr, T. M. (1993) *Biochemistry 32*, 14151−14157.
15. Takahashi, S., Wang, J., Rousseau, D. L., Ishikawa, K., Yoshida, T., Takeuchi, N., and Ikeda-Saito, M. (1994) *Biochemistry 33*, 5531−5538.
16. Hawkins, B. K., Wilks, A., Powers, L. S., Ortiz de Montellano, P. R., and Dawson, J. H. (1996) *Biochim. Biophys. Acta 1295*, 165−173.
17. Pond, A. E., Roach, M. P., Sono, M., Rux, A. H., Franzen, S., Hu, R., Thomas, M. R., Wilks, A., Dou, Y., Ikeda-Saito, M., Ortiz de Montellano, P. R., Woodruff, W. H., Boxer, S. G., and Dawson, J. H. (1999) *Biochemistry 38*, 7601−7608.
18. Hidaka, T., Omata, Y., and Noguchi, M. (1996) *Kurume Med. J. 43*, 313−324.
19. Omata, Y., Asada, S., Sakamoto, H., Fukuyama, K., and Noguchi, M. (1998) *Acta Crystallogr. D54*, 1017−1019.
20. Eliezer, D., and Wright, P. E. (1996) *J. Mol. Biol. 263*, 531−538.
21. Falzone, C. J., Mayer, M. R., Whiteman, E. L., Moore, C. D., and Lecomte, J. T. (1996) *Biochemistry 35*, 6519−6526.
22. Falzone, C. J., Wang, Y., Vu, B. C., Scott, N. L., Bhattacharya, S., and Lecomte, J. T. (2001) *Biochemistry 40*, 4879−4891.
23. Feng, Y., Sligar, S. G., and Wand, A. J. (1994) *Nat. Struct. Biol. 1*, 30−35.
24. Steller, I., Bolotovsky, R., and Rossmann, M. G. (1998) *J. Appl. Crystallogr. 30*, 1036−1040.
25. The CCP4 Suite: Programs for Protein Crystallography (1994) *Acta Crystallogr. D50*, 760−763.
26. Kabsch, W. (1998) *J. Appl. Crystallogr. 21*, 916−924.
27. Yeates, T. O. (1997) *Methods Enzymol. 276*, 344−358.
28. Brünger, A. T., Adams, P. D., Clore, G. M., DeLano, W. L., Gros, P., Grosse-Kunstleve, R. W., Jiang, J. S., Kuszewski, J., Nilges, N., Pannu, N. S., Read, R. J., Rice, L. M., Simonson, T., and Warren, G. L. (1998) *Acta Crystallogr. D54*, 905−921.
29. Britton, D. (1972) *Acta Crystallogr. A28*, 296−297.
30. Jones, T. A., Zou, J. Y., Cowan, S. W., and Kjeldgaard, M. (1991) *Acta Crystallogr. A47*, 110−119.
31. Laskowski, R. A., MacArthur, M. W., Moss, D. S., and Thornton, J. M. (1993) *J. Appl. Crystallogr. 26*, 283−291.
32. Chandra, N., Acharya, K. R., and Moody, P. C. E. (1999) *Acta Crystallogr. D55*, 1750−1758.
33. Redinbo, M. R., and Yeates, T. O. (1993) *Acta Crystallogr. D49*, 375−380.
34. Luecke, H., Richter, H. T., and Lanyi, J. (1998) *Science 280*, 1934−1937.
35. Zhou, H., Migita, C. T., Sato, M., Sun, D., Zhang, X., Ikeda-Saito, M., Fujii, H., and Yoshida, T. (2000) *J. Am. Chem. Soc. 122*, 8311−8312.
36. Ito-Maki, M., Ishikawa, K., Matera, K. M., Sato, M., Ikeda-Saito, M., and Yoshida, T. (1995) *Arch. Biochem. Biophys. 317*, 253−258.
37. Schuller, D. J., Zhu, W., Stojiljkovic, I., Wilks, A., and Poulos, T. L. (2001) *Biochemistry 40*, 11552−11558.
38. Zhu, W., Wilks, A., and Stojiljkovic, I. (2000) *J. Bacteriol. 182*, 6783−6790.
39. Baldwin, R. L. (1991) *Ciba Found. Symp. 161*, 190−205.
40. Nobbs, C. L., Watson, H. C., and Kendrew, J. C. (1966) *Nature 209*, 339−341.
41. Arnesano, F., Banci, L., Bertini, I., Faraone-Mennella, J., Rosato, A., Barker, P. D., and Fersht, A. R. (1999) *Biochemistry 38*, 8657−8670.
42. Muskett, F. W., Kelly, G. P., and Whitford, D. (1996) *J. Mol. Biol. 258*, 172−189.
43. Kraulis, P. J. (1991) *J. Appl. Crystallogr. 24*, 946−950.
44. Merritt, E. A., and Bacon, D. J. (1997) *Methods Enzymol. 277*, 505−524.

BI025662A